EUROPEAN ORGANIZATION FOR NUCLEAR RESEARCH
European Laboratory for Particle Physics

CERN EST/98-03 (LEA)
CERN ALICE/PUB 98-19

RADIATION STUDIES FOR THE ALICE ENVIRONMENT USING FLUKA AND ALIFE

A. Morsch and S. Roesler

Abstract

The ALIFE editor and parser for FLUKA geometries and input options is presented. The capabilities of ALIFE are demonstrated by radiation studies for the environment of the ALICE experiment at LHC. These studies cover beam-loss situations and induced radioactivity in the low-β insertions.

Presented at the Fourth Workshop on
Simulating Accelerator Radiation Environments, SARE4,
Knoxville, Tennessee, U.S.A.
September 14–15, 1998

CERN, Geneva, Switzerland
1 October 1998

I. INTRODUCTION

In the past, the accuracy of radiation studies based on Monte Carlo methods has often been limited by computer capacity. For calculations using the FLUKA code (see [1,2] and references therein) this has resulted in simplifying geometries, as the complexity of the geometry is related to computational time. The error on the results was often difficult to estimate.

Only recently very powerful workstation-clusters have become available allowing more detailed geometries to be simulated with a higher degree of accuracy. However, as the geometry becomes more complex, setting up, debugging and modifying the input for a FLUKA calculation becomes a more time-consuming task and often takes longer than the calculation itself. Moreover collaboration between different people working on a common input is almost impossible.

One possible solution is to construct an interface between a more appropriate language for developing complex geometries and the input read by FLUKA. Here we present the ALIFE editor and parser for FLUKA inputs and show how it has been successfully used for ALICE radiation calculations.

Two examples are discussed, both of which require a detailed consideration of different parts of the experimental environment:

a) Accidental beam loss: The radiation level in areas occupied by personnel (counting rooms, surface buildings) after an accidental beam loss depends crucially on the material distribution around the loss point as well as on the layout of caverns, shafts and shielding components. The calculations are based on a detailed FLUKA-geometry of the civil engineering and the low-β insertions at LHC Point 2 and of the ALICE detector.

b) Dose rates from induced radioactivity in the low-β insertions: Particles created in the very-forward or -backward directions of the proton-proton or nucleus-nucleus interactions may escape the detector and eventually interact in magnets of the low-β insertions producing radioactive isotopes. Dose rates from induced radioactivity are determined by the layout of detector and machine installations close to the beam as well as their magnetic fields.

II. THE MONTE CARLO SIMULATIONS

A. ALIFE: A geometry editor and parser for FLUKA

In a FLUKA calculation the three-dimensional space is divided into regions which each have different properties. The input to such a calculation therefore consists of two parts, a part defining the regions by combining geometrical bodies and a part which relates various options, parameters and cutoff-values to these regions. The region definitions have to be written in the language of the Combinatorial Geometry package. In the standard FLUKA input the bodies are numbered and are referred to in the region definitions by these numbers.

Many studies require the geometry to be defined in great detail. For example the geometry for the ALICE calculations described here consists of more than 900 bodies and 800 regions.

Developing and modifying geometries of this complexity in the conventional way is a very time-consuming task. For example, if a body is added to the list at a certain position or is removed from the list all bodies following the modified body-entry have to be renumbered, which means that also the numbers in the region definitions have to be changed correspondingly. Similarly if a region is split and the regions are renumbered sequentially then all subsequent assignments to the regions have to be altered.

ALIFE* is an interface between a more appropriate way of defining geometries and the input read by FLUKA. The geometry definition in the ALIFE "language" still consists of a list of bodies and regions. However in contrast to the conventional FLUKA geometry, bodies in ALIFE carry "names", i.e. labels consisting of up to eight letters, which are suitably chosen to remind one of the use of the body. In the region definitions the bodies are referred to by their names instead of by their numbers as in the standard FLUKA geometry definition. In this way the geometry input becomes much more "readable". Moreover the labels allow one to modify the list of bodies at any position since ALIFE takes care of the correct numbering. The following example has been taken from the geometry input for ALICE and should illustrate this philosophy:

Body definition:

```
* External void
EVOID RPP -999999.  999999.  -999999.  999999.  -999999.  999999.
* Cylinder around the geometry
EZYLI ZCC 0.0 0.0 10000.0
* Vertical planes to define the geometry
EPLN0 XYP -12000.0
EPLN1 XYP 12000.0
* Horizontal plane for the ground level
GROUN YZP 4482.0
```

Region definition:

```
* Air above the ground
>AIR:NF
BIASING=0.0, 1.0, .10000E5,
LOW-BIAS=72.0, 72.0, 0.7
+EZYLI-GROUN-EPLN0+EPLN1
```

This example also shows another feature of the ALIFE "language": Any parameter definition which refers to a certain region (such as the material of a region, biasing properties, etc.) is given at the same place in the input as the region definition. With this feature region numbers

*The name stands for "ALIce Fluka Editor" since it was initially developed for FLUKA calculations for the ALICE experiment. Of course, it can now be used to write the input for any FLUKA calculation. A detailed description can be found in the manual [3].

become obsolete and regions can be inserted or deleted at any place in the ALIFE input without renumbering.

ALIFE appears to the user as a graphical interface using windows and pull-down menus. The graphical interface allows to set up and modify the list of bodies. Furthermore it supports the user in debugging a geometry and in drawing sections through a geometry "on a mouse-click", i.e. it prepares the FLUKA input, executes FLUKA and shows the result in a separate window. Finally, the translation between the ALIFE format and the input required by FLUKA and vice versa is also controlled with pull-down menus.

Other features of ALIFE include the use of macros and global variables (for details see the manual [3]). They allow the replacement of certain parts of a geometry in a very convenient way, for example in order to study the effect of different shielding design options on the particle cascade. They also enable different users to work on a common geometry.

B. The FLUKA-geometry of LHC Point 2 (ALICE)

The use of ALIFE allowed to develop the geometries for the civil engineering, the ALICE detector and the low-β insertions separately at first. In particular, the FLUKA-geometry of the inner triplet was initially written for ATLAS radiation studies.[4] Due to the similarities of the low-β insertions at all LHC-intersection points this geometry could be adopted for the present calculations. In a second step the different parts were then combined to a single geometry.

The geometry is described in a right-handed orthogonal system with its origin at the ALICE interaction point, x as the vertical axis and y pointing towards the centre of the LHC ring.

A horizontal section through the FLUKA geometry at beam height is shown in Fig. 1 (left panel). Positions of shafts are indicated by dashed boxes. Vertical sections through the shafts are shown in Figs. 1 (right panel) and 2. All lines represent boundaries between different materials as used in the calculations.

Particle-backscattering from concrete walls of caverns and shafts has been taken into account by approximating the walls by a layer of concrete of a thickness of about 30 cm. The rock behind this layer has been treated as "black hole", *i.e.* as a region absorbing all particles which enter it.

The low-β insertions are located on either side of the interaction point starting at a distance of 23 m. The present geometry contains the inner quadrupole triplet (optics version 5) and the D1 separation/recombination dipole. Fig. 3 shows vertical transverse sections through the geometry of the magnets. ALIFE enables the user to superimpose the magnetic fields on the sections as can be seen in the figure.

C. Details of the FLUKA calculations

All calculations were carried out using FLUKA97.[1,2] In the following a few aspects of the calculations are summarized which are of importance to the radiation studies discussed fur-

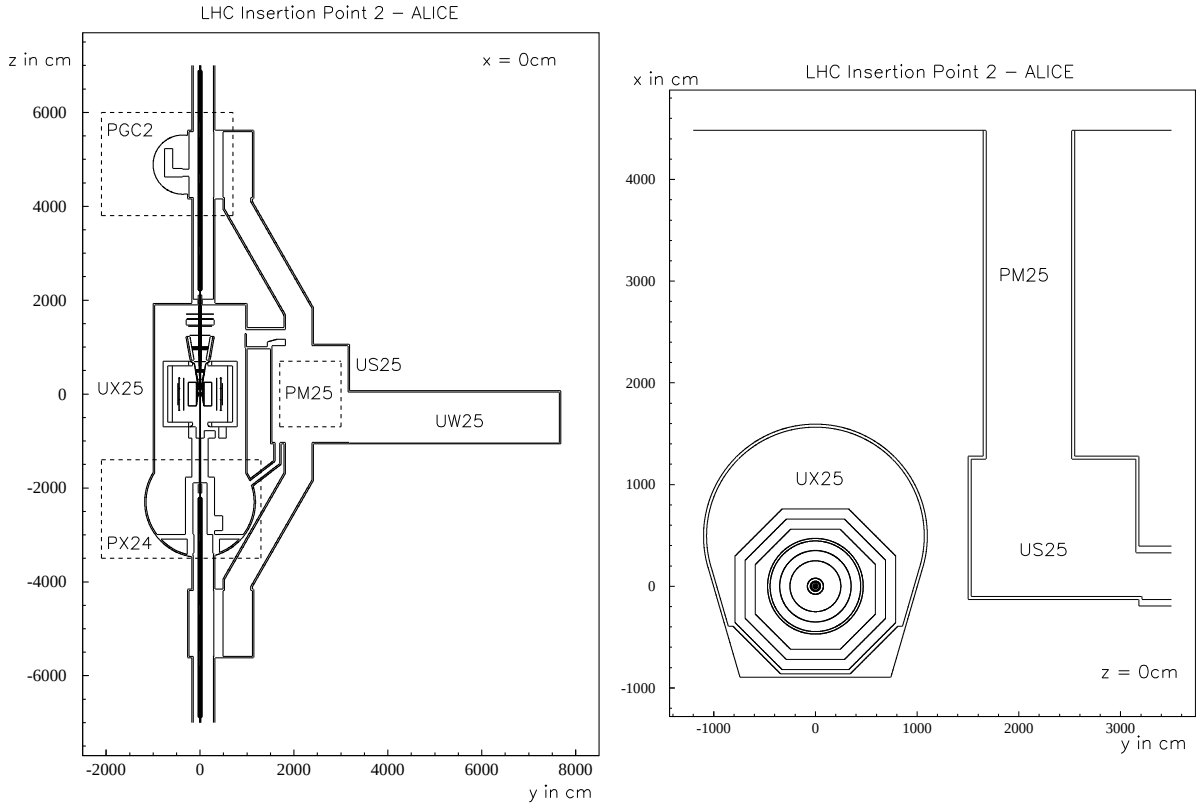

Figure 1: Left panel: Horizontal section through the geometry of LHC Point 2 at beam height ($x = 0$ cm). The locations of the vertical shafts PX24, PM25 and PGC2 are marked by dashed boxes. Right panel: Vertical transverse section through the interaction point and PM25 ($z = 0$ cm).

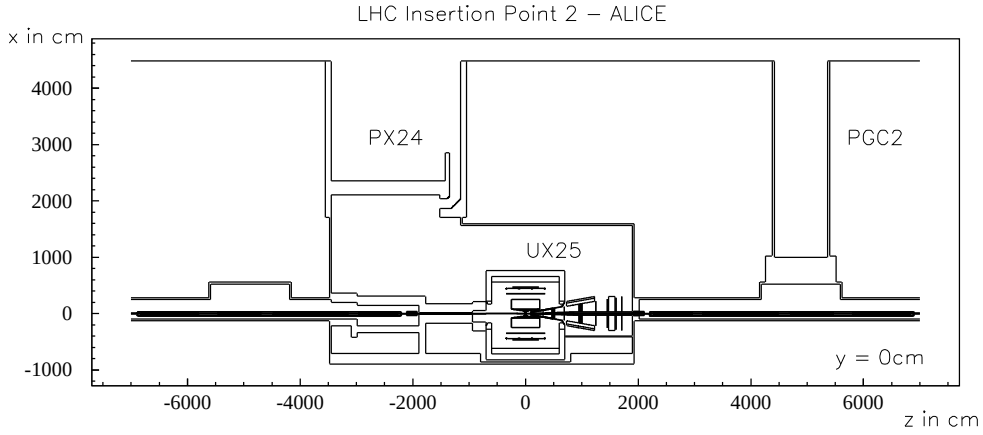

Figure 2: Vertical longitudinal section through the main experimental cavern UX25, the counting room shaft PX24 and the shaft PGC2.

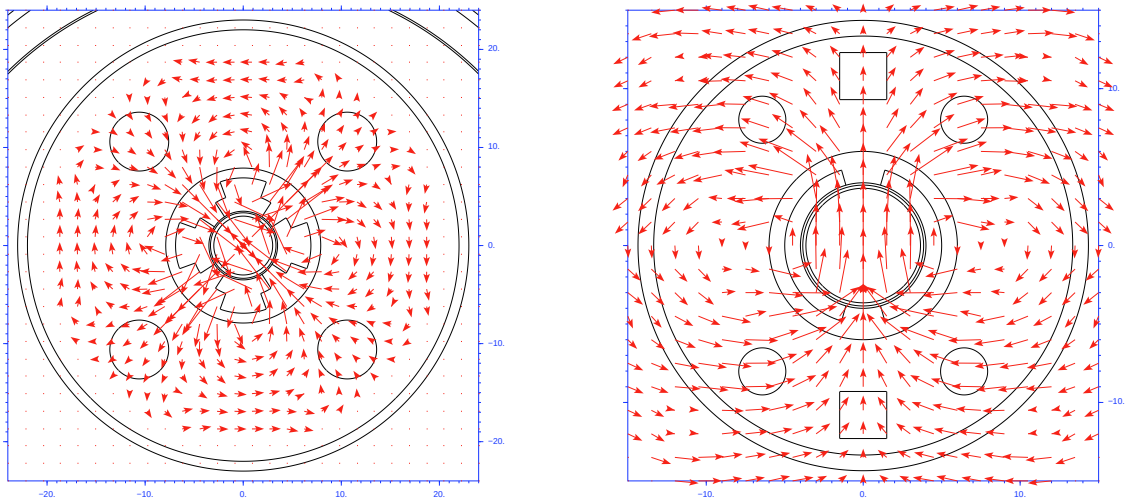

Figure 3: Vertical transverse sections through magnets of the low-β insertions. Arrows indicate magnetic field directions and relative strengths. Left panel: Quadrupole magnet of the inner triplet. Right panel: D1 dipole magnet.

ther below.

All concrete shielding components were assumed to have a density of 2.35 g/cm^3 and the following chemical composition (the values in brackets give the corresponding mass fractions): O (51.1%), Si (35.8%), Ca (8.6%), Al (2.0%), Fe (1.2%), H (0.6%), C (0.4%) and Na (0.3%).

In beam-loss studies lower thresholds for particle transport were set to 10 MeV for all hadrons except neutrons which were followed down to thermal energies. In order to keep the CPU-time within reasonable limits and still to obtain results of sufficient statistical significance the electromagnetic component of the particle cascade, which accounts for only up to 30% of the total dose equivalent,[5] was not calculated. Dose rates from induced radioactivity were calculated from densities of hadronic interactions (stars) whose primaries have energies larger than 50 MeV. Therefore in these calculations a 50 MeV cutoff was applied to the transport of all particles.

In the beam-loss studies significant use was made of region-importance biasing in order to enhance the statistical significance of the results in or behind regions of high attenuation.

Ambient dose equivalent due to neutrons, protons and charged pions has been directly derived from their fluences by multiplying the latter by energy dependent conversion factors.[6]

III. RESULTS OF RADIATION STUDIES

A. The radiation environment in beam-loss situations

At LHC Point 2 there are three shafts situated in the proximity of the collider (see also Figs. 1 and 2):

- PX24: The main access shaft, 23 m in diameter, provides a 15×15 m^2 opening for the installation of magnets and detector units and will accommodate the counting rooms of

the ALICE experiment. The LHC beam line will pass directly through the bottom part of the shaft.

- PM25: This shaft, 8.4 m in diameter, allows access to the machine bypass area and, via two access tunnels on either side of the ALICE detector, also a second access to the main experimental cavern.

- PGC2: The PGC2 shaft is located at the junction of the machine bypass tunnel and the beam tunnel and has a diameter of 12 m. The beam line of the LHC will pass close to the bottom part of this shaft.

Any accidental loss of the LHC beam causing exceptionally high radiation fields around the accelerator ring might also result in increased radiation levels in underground areas occupied by personnel and, via the three shafts, also above ground.

According to the CERN Radiation Safety Manual [7, 8] the counting room area in the PX24 shaft is classified as Controlled Radiation Area (maximum allowed ambient dose equivalent: 50 mSv), the surface areas around PX24 and PM25 are Supervised Radiation Areas (2.5 mSv) and the surface area around the PGC2 shaft is a Non-Designated Radiation Area (0.3 mSv).

Results of earlier radiation shielding studies for Point 2 can be found in [9, 10, 11, 12]. Here the use of ALIFE allowed for the first time to consider in the FLUKA calculations the effect of the detector and the inner triplet as well as of numerous details of shielding components and labyrinths. Further discussions on the results presented in this section can be found in [13].

1. The main access and counting room shaft PX24: The dose level in the counting room area above the shield plug depends strongly on the position of the loss point. "Worst case" scenarios can be expected if the beam is lost inside the inner triplet. Here, materials of rather high density are placed very close to the beam pipe and cause therefore a strong particle cascade. Beam losses inside the innermost quadrupole Q1 (lateral maximum of the cascade in the centre of the shaft) and in between the two lift shafts (leakage of radiation through the main shield plug *and* through the lift shafts) might lead to the highest dose values in the counting room area. Results based on a beam intensity of 4.7×10^{14} protons [14] are shown in Fig. 4. The dose equivalent values are well below the CERN-limits, even for areas of enhanced radiation such as above the ventilation duct. This conclusion still holds if a 30% contribution from electromagnetic cascades is added to the values given in the figure.

2. Radiation environment in the PM25 shaft: Increased radiation levels in the PM25 shaft might be caused if the LHC beam is lost at positions close to the entrances to the access tunnels which connect the machine bypass region US25 with the main experimental cavern UX25/PX24 (see Fig. 1, left panel). Since parts of the forward muon spectrometer provide significant lateral shielding the radiation streaming through the access tunnel between UX25 and US25 depends strongly on the exact location of the loss point. For the present design of the

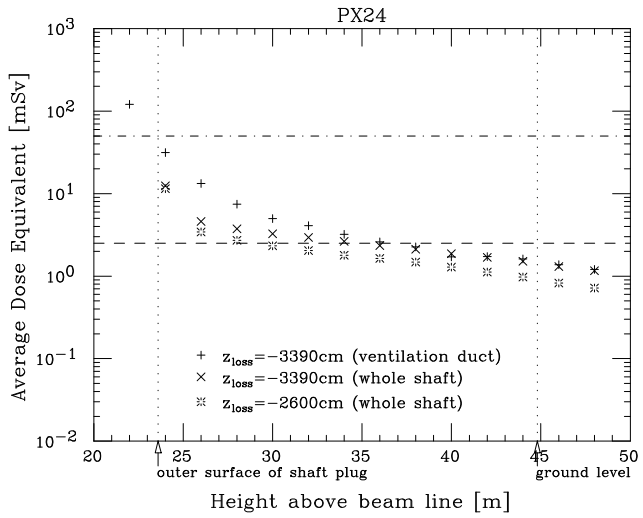

Figure 4: Ambient dose equivalent in the PX24 shaft shown for two different beam-loss positions. The position of the outer surface of the shaft plug and ground level are indicated by dotted lines. The design limits appropriate to Supervised Radiation Areas (2.5 mSv) and Controlled Radiation Areas (50 mSv) are indicated by dashed and dash-dotted lines, respectively.

detector [12] the radiation level is highest if the beam is lost in the lightly shielded section in between the magnet and the absorber. Figure 5 (left panel) shows dose equivalent values in the

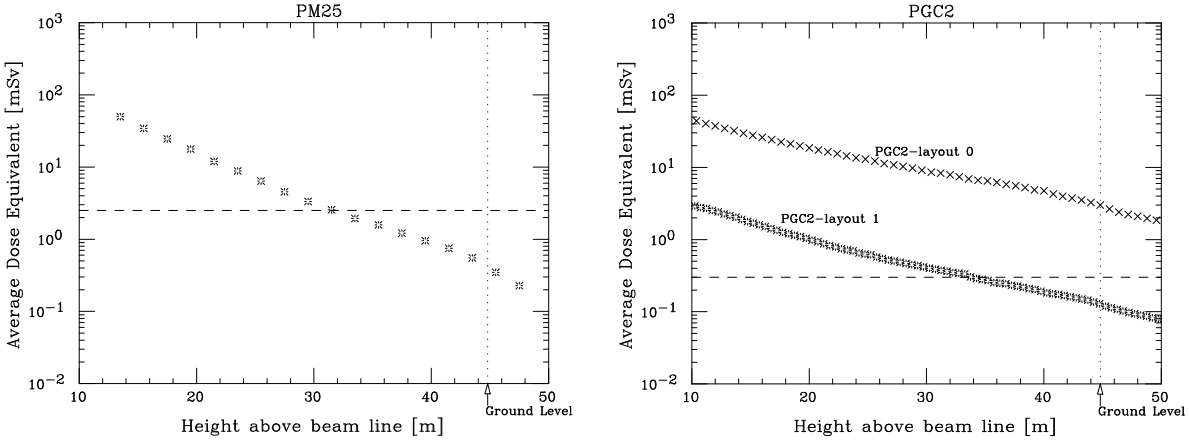

Figure 5: Ambient dose equivalent in the PM25 shaft (left panel; loss point: $z = 1400$ cm) and in the PGC2 shaft (right panel; loss point: $z = 4600$ cm). Dose equivalent constraints for ground level are indicated by dashed lines.

shaft caused by a loss at $z = 14$ m. As can be seen the dose equivalent values at ground level are lower than the CERN dose equivalent limit for Supervised Radiation Areas by a factor of four. The situation improves for losses close to the access tunnel between PX24 and US25 (not shown here, see [13] for details).

3. Radiation environment in the PGC2 shaft: In the case of a beam loss in the junction cavern UJ26 between the machine bypass and the beam tunnel the dose values inside PGC2, which is situated above this junction, might increase considerably due to two contributing sources:

(i) particle cascades penetrating the ceiling of UJ26 and (ii) radiation streaming through the access tunnel connecting PGC2 and UJ26. Two layouts for the ceiling and access tunnel have been studied and results are shown in Fig. 5 (right panel). The shielding requirements are not fulfilled for the initial layout ("Layout 0") as of Dec. 1987. We therefore propose a thicker concrete ceiling up to a level of 10 m above beam height and an extension to the labyrinth of the access tunnel ("Layout 1", see [13] for further details). With these modifications the dose equivalent above ground will be lower than the safety limit by at least a factor of 1.5 in any beam loss situation.

B. **Dose rates from induced radioactivity in the low-β insertions**

Realistic estimates of radioactivity induced by high energy secondary particles in low-β insertions and zero-degree calorimeters require a detailed consideration of installation and shielding components close to the beam pipe. In simulations particles have to be transported over long distances (up to 100 m) and any errors caused by approximations in the geometry may add up leading to considerable uncertainties in the results. The present study is an attempt to minimize these uncertainties by using ALIFE for the development of a detailed input to the FLUKA calculations.

In the following results are presented for proton-proton, calcium-calcium, and lead-lead collisions. These collisions were simulated using the DTUNUC event generator.[15,16] For individual nucleon-nucleon collisions DTUNUC is based on the PHOJET model [17,18] which allows the most sophisticated Monte Carlo description of diffractive proton-proton interactions known to us at present. [19] During event generation a beam crossing angle of 200 μrad for *pp* and 100 μrad for heavy ion collisions [20] has been taken into account.

The order of magnitude of the expected dose rate strongly depends on the interaction rate and the total energy of secondary particles hitting the magnets. First estimates can therefore be obtained from an inspection of these quantities (see Table 1).

Using the parameters as given in the table the interaction rates of *CaCa* and *PbPb* collisions differ from the *pp* interaction rate by factors of 3.3 and 0.1, respectively. To calculate the corresponding factors for the total energy only particles emerging the interaction within a pseudorapidity cone of a size of about $|\eta| > 4.6$ need to be taken into account since they are the only ones kinematically capable to reach the low-β insertions. The DTUNUC calculations yield factors of 11.0 and 46.0 for total energies in heavy ion collisions relative to *pp* collisions (Table 1). Assuming equal irradiation and cooling times the dose rates from *CaCa* and *PbPb* collisions can therefore be expected to be higher than the dose rate from *pp* interactions by factors of 36.3 and 4.6, respectively.

As these estimates show with the parameters of Table 1, dose rates will be highest for *CaCa* collisions. At present it is therefore sufficient to study only *CaCa* and *pp* collisions, the latter in order to verify the factor of 36.3 estimated above.

Table 1: Parameters used for the estimation of dose rates from induced radioactivity (from the top to the bottom): peak luminosity, luminosity averaged over 24-hours, inelastic cross section, resulting interaction rate, total energy of particles ($Z \leq 1$) with pseudorapidity $|\eta| > 4.6$, interaction rate relative to proton-proton collisions, total energy relative to proton-proton collisions, product resulting from multiplying the previous two lines.

		pp	*CaCa*	*PbPb*	Ref.
$\mathcal{L}_0$	[$\mathrm{cm}^{-2}\mathrm{s}^{-1}$]	10^{30}	10^{29}	10^{27}	[12]
$\langle\mathcal{L}\rangle_{24\mathrm{h}}$	[$\mathrm{cm}^{-2}\mathrm{s}^{-1}$]	5×10^{29}	5×10^{28}	5×10^{26}	[14]
σ_{inel}	[mb]	84	2850	7789	(DTUNUC)
$\langle R\rangle = \langle\mathcal{L}\rangle_{24\mathrm{h}} \times \sigma_{\mathrm{inel}}$	[s^{-1}]	4.2×10^4	1.4×10^5	3.9×10^3	
$E_{\mathrm{tot}}(\lvert\eta\rvert > 4.6)$	[TeV]	13.6	146.3	626.2	(DTUNUC)
$\langle R\rangle/\langle R\rangle_{\mathrm{pp}}$		1.0	3.3	0.1	
$E_{\mathrm{tot}}/E_{\mathrm{tot,\,pp}}$ $(\lvert\eta\rvert > 4.6)$		1.0	11.0	46.0	
		1.0	36.3	4.6	

There exist different approaches to estimate dose rates from induced radioactivity. The concept of ω-factors has been shown to provide reasonable first estimates for ferrous materials (see [21] and references therein) and is therefore also applied in the present study. It relates the dose rate to the density of inelastic interactions at energies above a certain energy threshold (usually 50 MeV), also called "star density".

In Fig. 6 the star density distributions in the D1-dipole magnets, the inner quadrupole triplets (Q1-Q3) and the corrector dipole magnets which will be installed in front of Q1 are shown for *CaCa* collisions and a horizontal section at beam height. The upper and lower panels show the distributions in backward and forward direction, respectively. There is yet no approved final design available for the corrector dipole magnet. [22] Therefore a standard warm dipole magnet has been assumed. The shielding layout in front of the corrector dipole essentially determines the star density in this dipole which is higher in backward direction. Apart from this difference the distributions in forward and backward directions are comparable. There is a slight horizontal asymmetry in the distribution in D1 which is due to the magnetic field bending particle tracks sidewards.

Star density values for locations inside the magnets close to the beam pipe (radius: $4 \leq r \leq 5$ cm) are shown in Fig. 7. Here the azimuthal maximum value is given as function of the distance from the interaction point. Histograms represent star densities calculated with FLUKA using particles produced in *pp* and *CaCa* collisions as generated with DTUNUC. In order to verify the scaling factors discussed above and to obtain estimates for *PbPb* collisions star densities for *pp* collisions have been scaled to *CaCa* and *PbPb* collisions with the factors

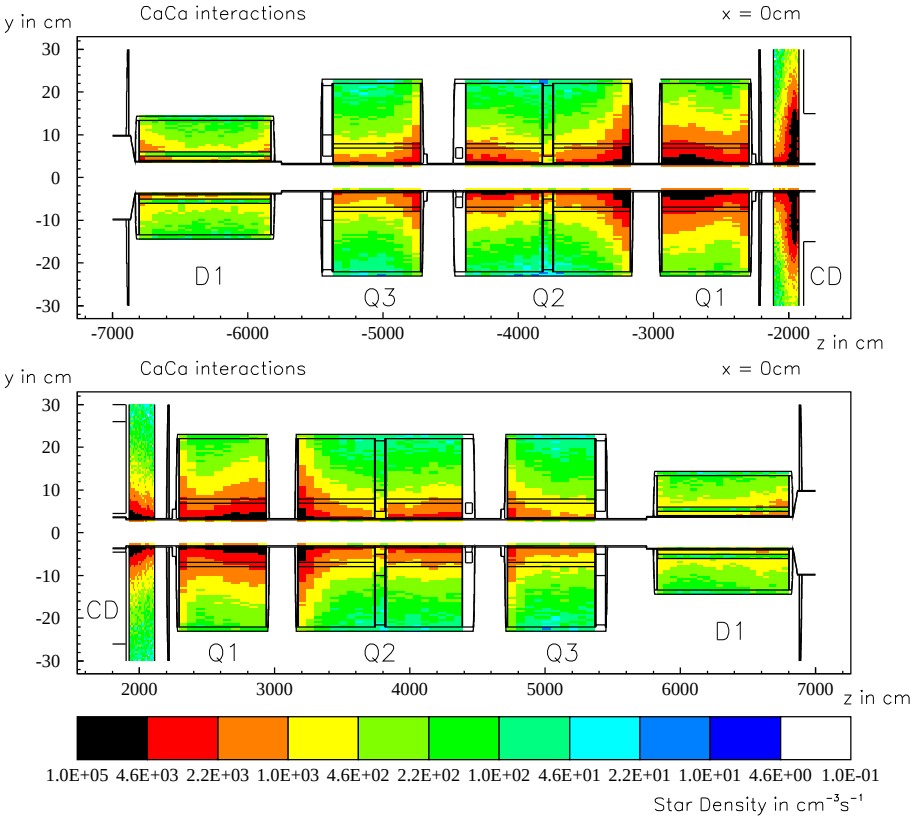

Figure 6: Star density distributions in magnets of the low-β insertions and in the corrector dipole magnets in calcium-calcium collisions. The distributions given for a horizontal section at beam height are shown for the backward (upper panel) and forward (lower panel) directions separately.

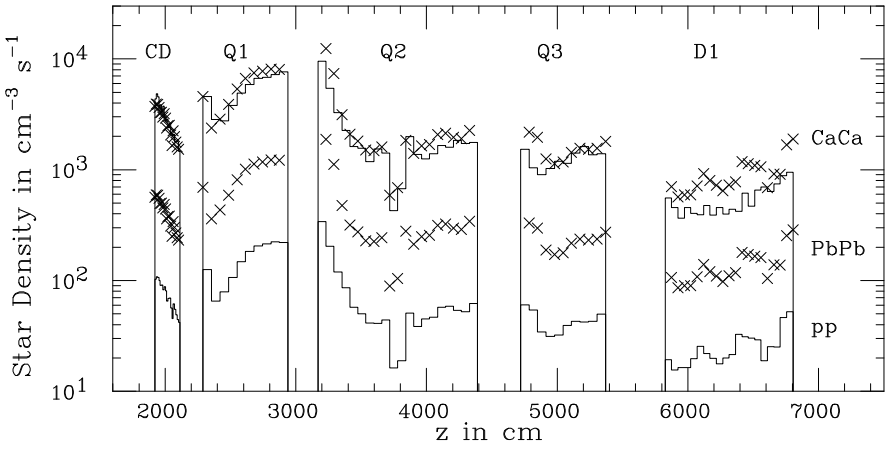

Figure 7: Star densities in magnets of the forward low-β insertion (Q1-Q3,D1) and in the corrector dipole (CD). Shown is the azimuthal maximum value averaged over a distance from the beam between 4 and 5 cm. Star densities calculated for *pp* and *CaCa* collisions are given as histograms. Crosses show the star density for *pp* collisions scaled to *CaCa* and *PbPb* collisions with the factors given in the last line of Table 1.

given in the last line of Table 1. Results are shown in Fig. 7 as crosses. It is evident that the scaling method provides a rather accurate estimate and justifies our approach of estimating dose rates for *PbPb* collisions without performing explicit FLUKA calculations for this case.

Dose rates can be derived from the star density distributions either by multiplying them directly with an ω-factor of the order of 10^{-8} Sv h^{-1}/(cm^{-3}s^{-1}) ("contact dose rate") or by using the FIASCO code.[23] The approach implemented in FIASCO is also based on the ω-factor concept but takes in addition photon build-up and attenuation into account. In both cases results are obtained for 30 days of irradiation and one day of cooling time. For the present study FIASCO has been used.

Results for *CaCa* collisions are presented in Fig. 8. The left panel shows dose rates at

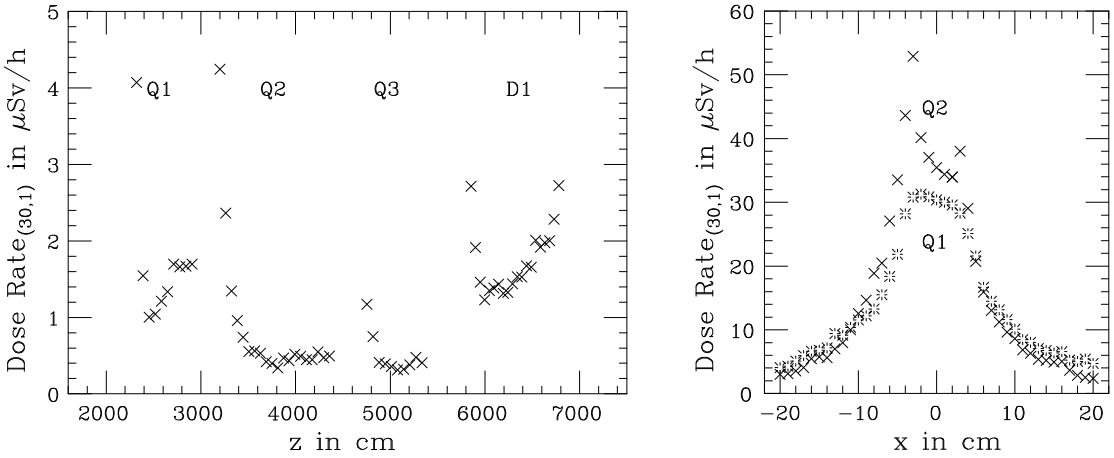

Figure 8: Dose rates from induced radioactivity in *CaCa* collisions. Left panel: Dose rates at the outer surface of the coils of the forward inner triplet ($x = -23$ cm, $y = 0$ cm) and D1-dipole magnet ($x = 0$ cm, $y = 14.35$ cm). Right panel: Dose rates at the front plates of the Q1- ($y = 0$ cm, $z = 2290$ cm; stars) and the Q2-yokes ($y = 0$ cm, $z = 3170$ cm; crosses).

the outer surface of the inner triplet and D1-yokes. The magnetic field in the forward muon spectrometer bends particle tracks downwards. Therefore highest dose rates can be expected underneath the inner triplet for which locations dose rates are shown in the figure. In contrast, the magnetic field of D1 bends particle tracks horizontally causing highest dose rates at the side of D1 which points towards the centre of the LHC-ring. For the D1-dipole the z-dependence is therefore shown for beam height and $y = 14.35$ cm (outer surface of the yoke).

The right panel of Fig. 8 shows dose rates at the front plate of Q1 and Q2. Here the variation with x is shown ($y = 0$ cm) which contains the maximum value for the corresponding front plate. Again, the asymmetry in x is caused by the magnetic field of the muon spectrometer.

IV. CONCLUSIONS

The ALIFE editor and parser for FLUKA geometries and input options allows one to develop and modify complex geometries in a very efficient way. Its modular structure for geometry definition enables different users to work on a common geometry.

ALIFE has been successfully used for radiation calculations for the ALICE environment at the LHC. Two aspects were studied, both of which required a detailed FLUKA geometry of different parts of the experiment and installations at Point 2 of the LHC.

Radiation shielding calculations for accidental beam-loss situations showed that with the present design of the beam shield and the shield plug the radiation level around PX24 stays below the CERN limits for the counting rooms as a Controlled Radiation Area and the surface area as a Supervised Radiation Area. Furthermore the access tunnels between the main experimental cavern and the machine bypass area provide sufficient shielding for the surface area above PM25 also to be classified as Supervised Radiation Area. In contrast the present design of the shielding at the bottom of PGC2 is not sufficient and has to be modified in order to meet the radiation safety requirements for the surface area above PGC2.

The use of ALIFE also allowed rather detailed studies of dose rates from induced radioactivity in the low-β insertions during normal collider operation. With the luminosities for proton-proton and heavy ion collisions as presently planned the calcium-calcium collider option leads to the highest dose rates in installations close to the beam. The results show that the dose rates from induced radioactivity will not create handling difficulties in the machine area.

ACKNOWLEDGEMENTS

We would like to thank Galina Chabratova, Ian Dawson, Lars Leistam, Blahoslav Pastircak, Graham Stevenson, Heinz Vincke and Sylvain Weisz for many useful discussions and Graham Stevenson for comments on the manuscript.

We are also grateful to Alberto Fassò and Alfredo Ferrari for providing the FLUKA code.

REFERENCES

1. A. Ferrari, T. Rancati and P. R. Sala, *FLUKA applications in high energy problems: from LHC to ICARUS and atmospheric showers*. In *Proceedings of The Third Workshop on Simulating Accelerator Radiation Environments (SARE-3)*, KEK, Tsukuba, Japan, 1997, p. 165, 1997.
2. A. Fassò, A. Ferrari, J. Ranft and P. R. Sala, *New developments in FLUKA modelling of hadronic and EM interactions*. In *Proceedings of The Third Workshop on Simulating Accelerator Radiation Environments (SARE-3)*, KEK, Tsukuba, Japan, 1997, p. 32, 1997.
3. A. Morsch, *ALIFE: A Geometry Editor and Parser for FLUKA*. ALICE Internal Note/SIM, ALICE/98–29 (http://www.cern.ch/alice/Projects/offline/Simulation/fluka/) (1998).
4. I. Dawson and G. R. Stevenson, *Radiation studies in the collimator regions of the ATLAS experimental area*. CERN Internal Report TIS–RP/IR/98–01 (1998).
5. H. Nakashima, M. Huhtinen and G. R. Stevenson, *Estimations of the shielding wall thickness for the LHC-B detector*. CERN Internal Report TIS–RP/IR/96–30 (1996).
6. A. V. Sannikov and E. N. Savitskaya, *Ambient dose and ambient dose equivalent conversion factors for high-energy neutrons*. CERN Divisional Report TIS–RP/93–14/PP (1993).

7. M. Höfert and G. R. Stevenson, *Design limits for doses and dose rates for beam operation at the LHC*. CERN Internal Report TIS–RP/IR/95–04 (1995).
8. Radiation Protection Group, *Radiation Safety Manual 1996*, CERN (1996).
9. G. Chabratova, W. Klempt, L. Leistam and N. Slavin, *The radiation environment of the ALICE experiment*. ALICE Internal Note, ALICE/95-41 (1995).
10. G. Chabratova and L. Leistam, *Estimation of the radiation environment and the shielding aspects for the Point 2 area of the LHC*. (1997).
11. E. Wallén and G. R. Stevenson, *Shielding properties of the PGC2 shaft at the ALICE experiment*. CERN Internal Report TIS–RP/IR/97–13 (1997).
12. The ALICE Collaboration, *Technical proposal for a large ion collider experiment at the CERN LHC*. CERN/LHCC/95-71 (1995).
13. S. Roesler and G. R. Stevenson, *The radiation environment at the LHC intersection point 2 (ALICE) in beam loss situations*. CERN Internal Report TIS–RP/IR/98–10 (1998).
14. K. Potter and G. R. Stevenson, *Average interaction rates for shielding specification in high-luminosity LHC experiments*. CERN Internal Report TIS–RP/IR/95–05 (1995).
15. R. Engel, J. Ranft and S. Roesler, *Photoproduction off nuclei and point-like photon interactions, Part I: Cross sections and nuclear shadowing*. Phys. Rev. D55 (1997) 6957.
16. S. Roesler, R. Engel and J. Ranft, *Photoproduction off nuclei: Particle and jet production*. Phys. Rev. D57 (1998) 2889.
17. R. Engel, *Photoproduction within the two-component Dual Parton Model: Amplitudes and cross sections*. Z. Phys. C66 (1995) 203.
18. R. Engel and J. Ranft, *Hadronic photon-photon interactions at high energies*. Phys. Rev. D54 (1996) 4244.
19. F. W. Bopp, R. Engel and J. Ranft, *Rapidity gaps and the* PHOJET *Monte Carlo*. BA-98-17, e-Print Archive: hep-ph/9803437 (1998)
20. The LHC Study Group, *LHC - The Large Hadron Collider, Conceptual Design*. CERN/AC/95-05 (LHC) (1995).
21. R. H. Thomas and G. R. Stevenson, *Radiological Safety Aspects of the Operation of Proton Accelerators*. Technical Reports Series No. 283, International Atomic Energy Agency, Vienna, 1988.
22. L. Leistam, private communication, 1998.
23. M. Huhtinen, *Method for estimating dose rates from induced radioactivity in complicated hadron accelerator geometries*. CERN Internal Report TIS–RP, in preparation.